LASER & PHOTONICS REVIEWS

www.lpr-journal.org

Multimode Waveguide Bends in Lithium Niobate on Insulator

Mingyang Ma, Mingrui Yuan, Xudong Zhou, Huifu Xiao, Pengfei Cao, Lin Cheng, Thach Giang Nguyen, Andreas Boes, Guanghui Ren,* Yikai Su, Arnan Mitchell, and Yonghui Tian**

Lithium niobate on insulator (LNOI) is a promising platform for realizing high-performance photonic integrated circuits (PICs) for communication applications due to LN's excellent electro-optic properties. Multimode photonic devices are attractive as they can improve the communication capacity of PICs by multiplexing orthogonal modes. For connecting multimode photonic components on the same chip, multimode waveguide bends are indispensable. In this contribution, multimode waveguide bends are proposed, simulated, and experimentally demonstrated with double air grooves to ensure low crosstalk for three different transverse electric (TE) modes by improving the mode overlap at the interface between the straight and bent waveguide when the waveguide is bent. This enables demonstration of S-shaped waveguide bends (two 90° bent waveguides) with insertion losses below 1.42, 1.12, and 2.5 dB in the wavelength range of 1525–1575 nm for the transmitted TE_0, TE_1, and TE_2 modes, respectively. The mode crosstalk is lower than −12.2 dB for all three modes. The demonstrated device provides a compact solution for multimode waveguide bends in the LNOI platform, paving the way for high-speed, high-data-capacity PICs for on-chip communication systems.

1. Introduction

Photonic integrated circuits (PICs) with various active and passive circuit components integrated on a single chip can be used for high-speed and large-capacity information communication systems. Lithium niobate on insulator (LNOI) has the potential to play an important role in the development of high-speed and large-data-capacity PICs thanks to its excellent electro-optic properties,[1–5] low loss, and wide transparency window. The attractive properties have enabled the demonstration of a series of high-speed active circuit components in LNOI, such as electro-optical switches,[6,7] modulators,[8] and tunable filters,[9] which can be connected with passive circuit components such as polarization division multiplexers, mode division multiplexers (MDMs),[10] reflection filter,[11] microring resonator,[12] Y-splitters[13] to make full use of them. Although many passive circuit components have already been experimentally demonstrated,[14–17] some still remain to be investigated, such as multimode waveguide bends, which are needed to connect MDMs for high-data-capacity PICs in LNOI.

Multimode waveguide bends can change the propagation direction of multiple optical modes with low loss and low inter-mode crosstalk. Such bends need to be carefully designed, as

M. Ma, P. Cao, L. Cheng
Institute of Optoelectronics & Electromagnetic Information
School of Information Science and Engineering
Lanzhou University
Lanzhou, Gansu 730000, China
E-mail: chenglin@lzu.edu.cn

M. Yuan, X. Zhou, H. Xiao, Y. Tian
School of Physical Science and Technology
Lanzhou University
Lanzhou, Gansu 730000, China
E-mail: siphoton@lzu.edu.cn

T. G. Nguyen, A. Boes, G. Ren, A. Mitchell
Integrated Photonics and Applications Centre (InPAC)
School of Engineering
RMIT University
Melbourne, VIC 3001, Australia
E-mail: guanghui.ren@rmit.edu.au

A. Boes
School of Electrical and Electronic Engineering
The University of Adelaide
Adelaide, SA 5005, Australia

A. Boes
Institute for Photonics Advanced Sensing
The University of Adelaide
Adelaide, SA 5005, Australia

Y. Su
The State Key Laboratory of Advanced Optical Communication Systems and Networks
Department of Electronic Engineering
Shanghai Jiao Tong University
Shanghai 200240, China

The ORCID identification number(s) for the author(s) of this article can be found under https://doi.org/10.1002/lpor.202200862

DOI: 10.1002/lpor.202200862

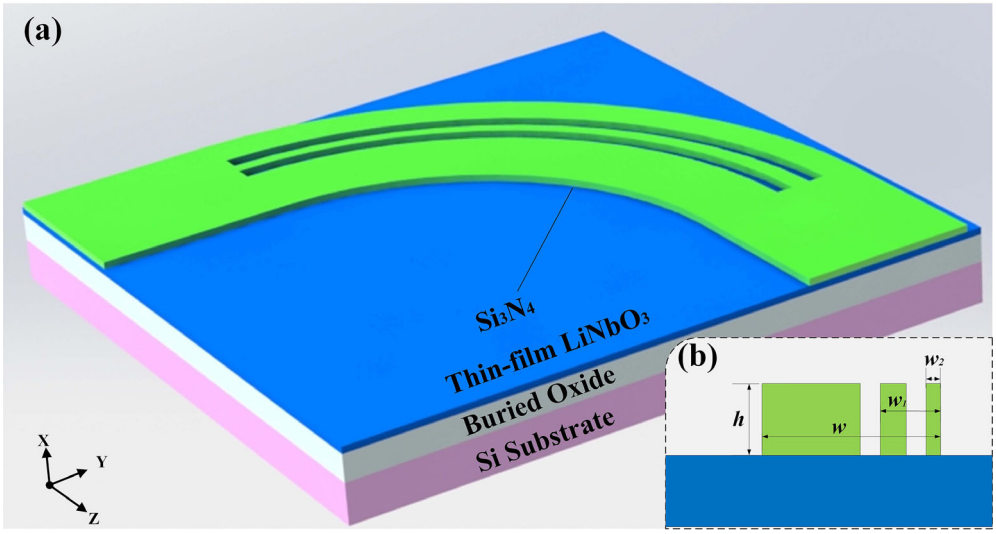

Figure 1. a) The schematic diagram of the proposed multimode waveguide bend, b) cross-section view of the multimode waveguide bending.

mode crosstalk can occur at the interface between straight and bent waveguides due to the mismatch of the optical modes,[18] which causes crosstalk and degrades the transmission performance of the multimode optical signals. To reduce the crosstalk among the modes in multimode waveguide bends, various schemes have been reported in the Silicon-on-Insulator (SOI) platform, such as Euler bends,[19–22] optical transformation,[23] shallow etched grating assistance,[24] and inverse design.[25,26] However, to the best of our knowledge, no multimode waveguide bends have been reported in the LNOI platform.

In this contribution, we propose, simulate, and experimentally demonstrate multimode waveguide bends that support three different transverse electric (TE) modes (TE_0, TE_1, and TE_2) in the LNOI platform with compact size, low loss, and low crosstalk. This is achieved by using two air grooves in the multimode waveguide bends. Experimental results show that the insertion loss of TE_0, TE_1, and TE_2 modes propagating in a pair of 90° multimode waveguide bends is below 1.42, 1.12, and 2.5 dB, respectively, in a wavelength range of 1525–1575 nm. The mode crosstalk is less than −12.2 dB for the three modes. In addition, the cut-back method is used to estimate the insertion loss for a single 90° multimode waveguide bend at 1550 nm, which is 0.39, 0.29, and 0.85 dB for the TE_0, TE_1, and TE_2 modes, respectively. The demonstrated multimode waveguide bends provide an efficient solution for interconnecting multimode photonic circuit components on a single chip, paving the way for high-data-capacity multimode PICs in the LNOI platform.

2. Design and Working Principle

For the investigation of the multimode waveguide bends we use the silicon nitride (Si_3N_4) loaded LNOI waveguide platform, where the Si_3N_4 on top of the LN thin film is patterned to achieve the horizontal confinement of optical modes.[10] As a common optical loading material on the LNOI platform, Si_3N_4 has a similar but slightly lower refractive index and similar transparency window to LN, and more importantly, it can be deposited and patterned by the mature fabrication processes that have been developed in CMOS foundries. This platform uses the mature Si_3N_4 fabrication process while the waveguide design results in most of the optical field being confined in the LN layer,[10,27–29] taking full advantage of LN's attractive properties. **Figure 1**a shows a schematic diagram of the 90° multimode waveguide bend formed by a circular curved waveguide with two similar curved air grooves. For our design, we choose an X-cut LNOI platform with the thicknesses of the LN and Si_3N_4 layers of both 300 nm, consistent with our previous work.[30] The radius of the proposed multimode waveguide bend is 120 μm to ensure a compact size and the width is 4.48 μm to support the TE_0, TE_1, and TE_2 modes. The waveguide bend has two circular curved air grooves with a width of 120 nm and a height of 300 nm, as shown in Figure 1a. The cross-section of the proposed multimode waveguide bend is shown in Figure 1b with the specific structural parameters marked as h, w, w_1, and w_2 respectively.

The working principle of the proposed multimode waveguide bend is described as follows: When optical modes pass from the straight waveguide to the multimode waveguide bends, intermode crosstalk occurs due to the modal mismatch between the straight and bent waveguide. To reduce the modal crosstalk in the bend, we introduce two air grooves with a width of 120 nm and a height of 300 nm (Si_3N_4 is fully etched), as shown in Figure 1a. This allows us to manipulate the effective index gradient of the waveguide in the radial direction,[18] so that the optical modes experience a lower effective refractive index at the outer edges of the bend. As a result, the mode distribution in the waveguide bend is manipulated in a way that reduces the modal mismatch between the straight and bent waveguide, reducing the modal crosstalk.

To achieve low crosstalk, we calculated the modal overlap for the straight and bent waveguide using a finite difference eigenmode (FDE) solver.[31] The calculation results are shown in **Figure 2**a–c, in which the horizontal and the vertical axis are related to the structure parameters w_1 and w_2 labeled in Figure 1b. Assuming $w_1 = m*l$, $w_2 = n*l$, n and m are constants that are greater than 1 and only one decimal place such as 1.1, 1.2, 1.3, etc., and l

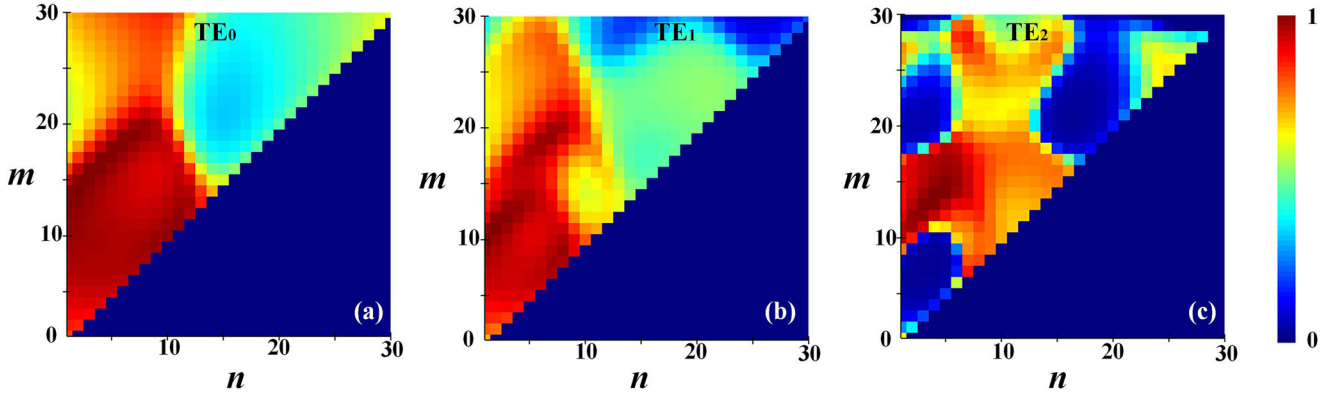

Figure 2. The modal overlap integral of a) TE_0 mode, b) TE_1 mode, and c) TE_2 mode.

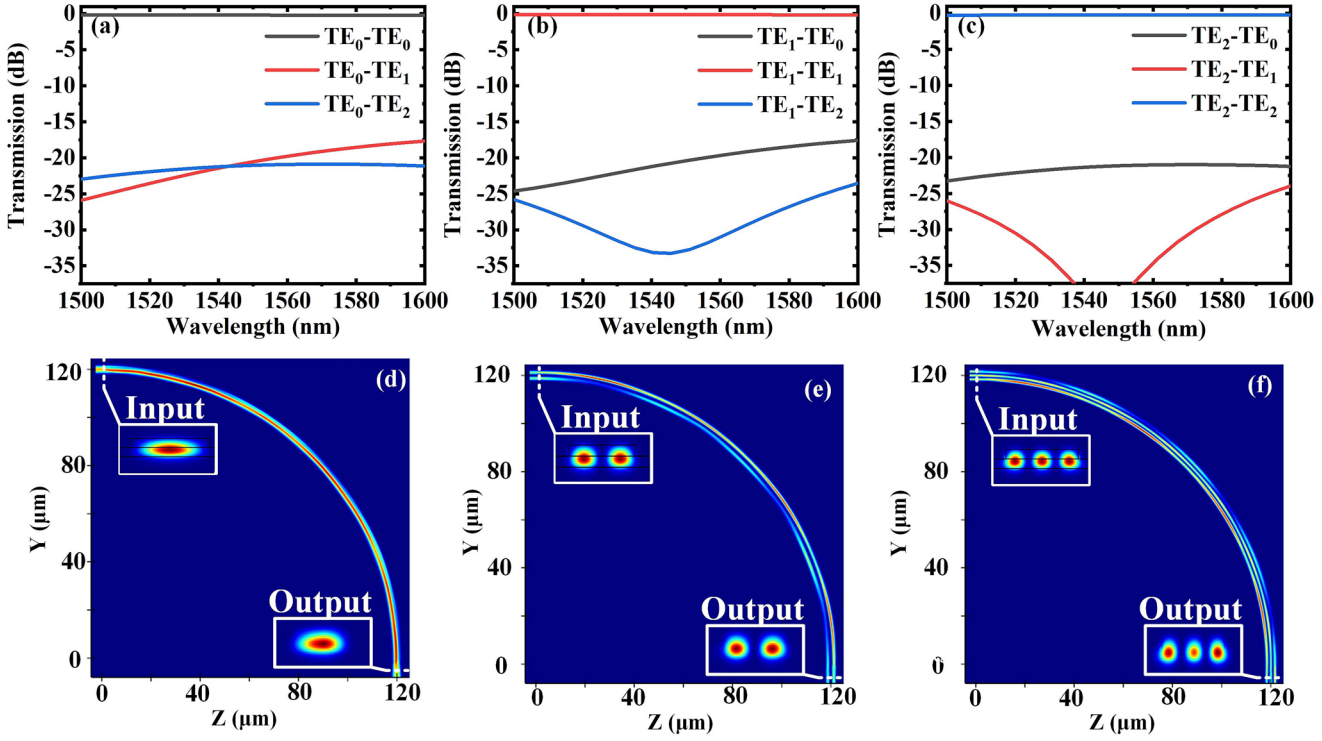

Figure 3. The simulated transmission spectra for a) TE_0 input, b) TE_1 input, and c) TE_2 input; The simulated field distribution for d) TE_0 input, e) TE_1 input, and f)TE_2 input.

is chosen as 100 nm by considering the fabrication accuracy. According to Figure 2, the modal overlap integrals for TE_0, TE_1, and TE_2 mode are optimal when $n = 3.7$ and $m = 15$, therefore, $w_1 = 1500$ nm, $w_2 = 370$ nm are determined and the overlap integral values of the three modes are 0.95, 0.917 and 0.932, respectively.

The finite difference time domain (FDTD) method is used to simulate the transmission performance of the multimode waveguide bend by the determined structure parameters $h = 300$ nm, $w = 4.48$ μm, $w_1 = 1.5$ μm, and $w_2 = 370$ nm. The simulated results are shown in **Figure 3**, from which we can see the insertion losses are below 0.22, 0.18, and 0.25 dB for TE_0, TE_1, and TE_2 respectively, and the inter-modal crosstalk is less than −17.5 dB in the wavelength range of 1500–1600 nm. Figure 3d–f shows the simulated field distribution of the proposed multimode waveguide bend when TE_0, TE_1, or TE_2 is launched from the input port, respectively, from which we can see these three optical modes can propagate in the proposed multimode waveguide bend with low loss and low inter-mode crosstalk as expected.

For comparison, we simulate the transmission of the multimode waveguide bend with the same dimensions, but without the additional air grooves. The simulated transmission spectra of the common multimode waveguide bend are presented in

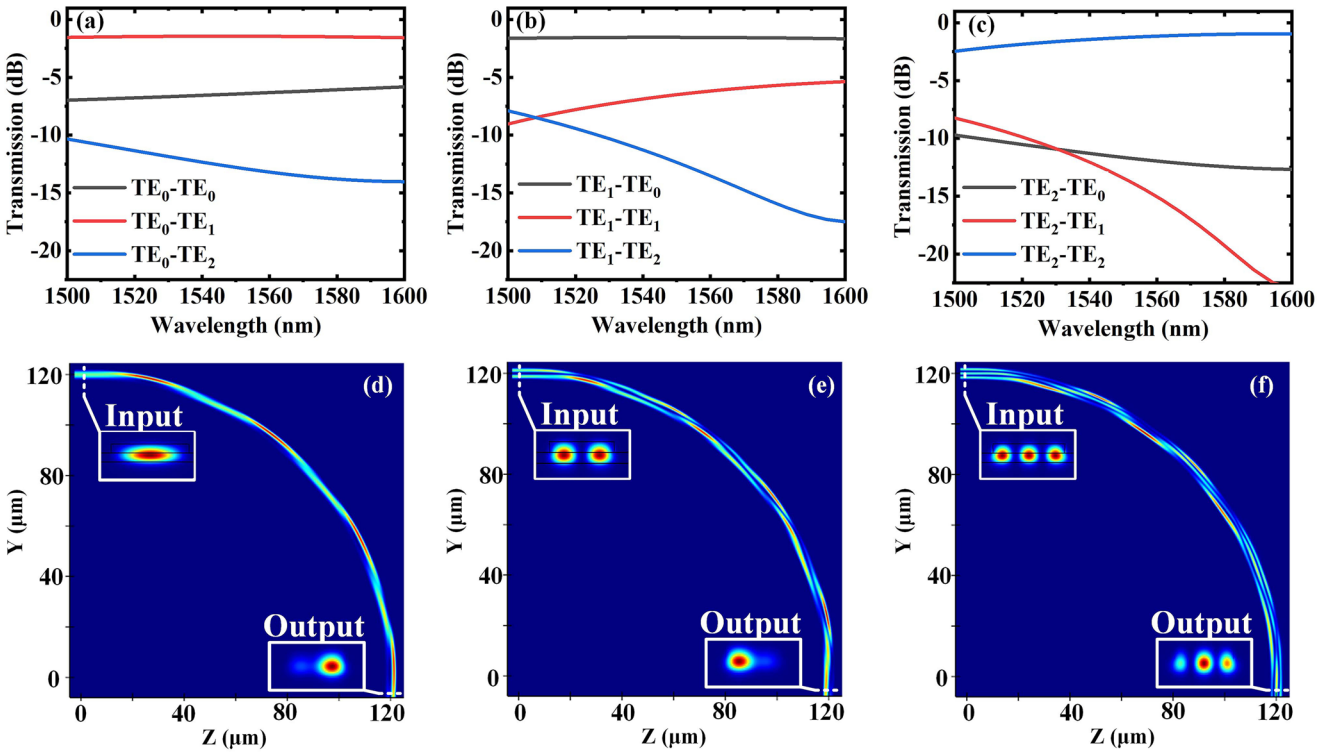

Figure 4. The transmission spectra of a multimode waveguide bend without air grooves for a) TE_0 input, b) TE_1 input, and c) TE_2 input. The simulated field distribution of a multimode waveguide bend without air grooves for d) TE_0 input, e) TE_1 input, and f) TE_2 input.

Figure 4a–c, from which we can see that the insertion loss and inter-mode crosstalk are degraded compared to the multimode waveguide bend with air grooves. The simulated field distribution shown in Figure 4d–f indicates that the modal mismatch of the multimode waveguide bend is significant. This demonstrates that our proposed multimode waveguide bend with air grooves reduces the transmission loss and inter-mode crosstalk strongly.

3. Experimental Results

Next, we fabricated the multimode waveguide bend for experimental verification. For this, we used a commercial X-cut LNOI wafer with a 4.7 μm-thick buried oxide and a 300 nm-thick LN thin film, on which we deposited a Si_3N_4 thin film layer with a thickness of 300 nm.[10] Afterwards we used electron beam lithography (EBL) and inductively coupled plasma (ICP) etching processes to pattern the Si_3N_4 and form the waveguides. To characterize the multimode waveguide bend, we used a pair of 3-channel MDMs with grating couplers on either side of the bends, which enabled us to excite the modes of interest in the multimode waveguide.

An optical microscope image of the fabricated multimode waveguide bend and multimode straight waveguide (reference waveguide) is shown in **Figure 5**a. The fabricated multimode waveguide bends had an S-bend formed by two cascaded bends. We investigated bends with air grooves and without air grooves for comparison. The scanning electron microscope (SEM) images of the fabricated multimode waveguide bend with different magnifications are shown in Figure 5b, c.

We used a broadband light source (1525–1575 nm) and an optical spectrum analyzer (OSA) to characterize the fabricated multimode waveguide bends. The light from the broadband light source is first coupled into the device using the grating couplers, and the output light is connected to the OSA for observing the transmitted optical spectrum. To eliminate the effects of the MDMs and remove the spectral dependence of the grating coupler efficiency, we normalized all experimental results with the reference straight multimode waveguide (shown in Figure 5a). **Figure 6**a–c shows the experimental results of the fabricated device including two 90° multimode waveguide bends, from which we can see the insertion losses are about 1.4, 1.1, and 2.5 dB for the modes TE_0, TE_1, and TE_2 respectively. The inter-mode crosstalk in the investigated wavelength range is less than −12.2 dB for all the modes. To characterize the performance of the proposed multimode waveguide bends more accurately, we fabricated devices with 0, 2, 4, 6, 8, and 10 cascaded multimode waveguide bends. Figure 6d–f shows the transmission as a function of the number of bends. By linear fitting, we can extract the insertion loss of the bend for the different modes, which were 0.39, 0.29, and 0.85 dB for TE_0, TE_1, and TE_2 modes at the wavelength of 1550 nm. If we compare this with the simulated results, we find that the performance of the fabricated device is slightly degraded, especially in terms of inter-mode crosstalk, which may be caused by fabrication variations of the fabricated devices. As shown in **Figure 7**, we investigate the transmission response of our device to the fabrication variations of the slot width by performing the 3D FDTD simulations. It can be seen that for TE_0, TE_1, and TE_2 modes, the crosstalk increases when the slot widths increase or decrease by 20 nm. However, we can also find that the experimental crosstalk is still lower than −12.2 dB within a bandwidth of 100 nm, which indicates that the device is tolerant to slot width variations.

For comparison, we also included the results for S-bend multimode waveguide bends without air grooves. The corresponding spectra for different input modes are shown in **Figure 8**a–c, from which we can see the insertion loss and crosstalk of the not optimized multimode waveguide bends is degraded greatly in the wavelength range of 1525–1575 nm. This indicates that the proposed multimode waveguide bends are effective to realize bends with a tight bending radius, while maintaining low loss and low inter-modal crosstalk.

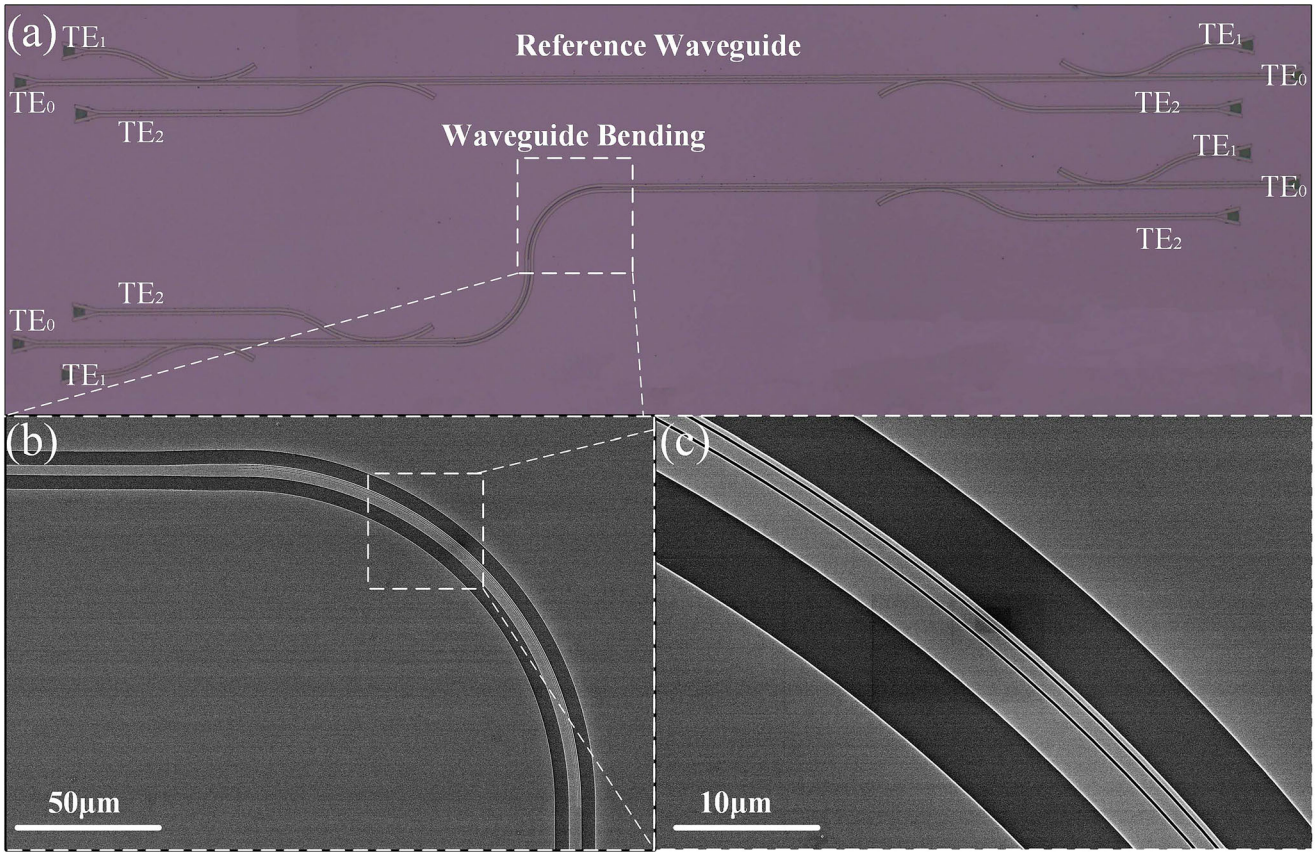

Figure 5. a) Optical microscope image of the fabricated multimode waveguide bend. b,c) SEM images of the proposed multimode waveguide bends with different magnifications.

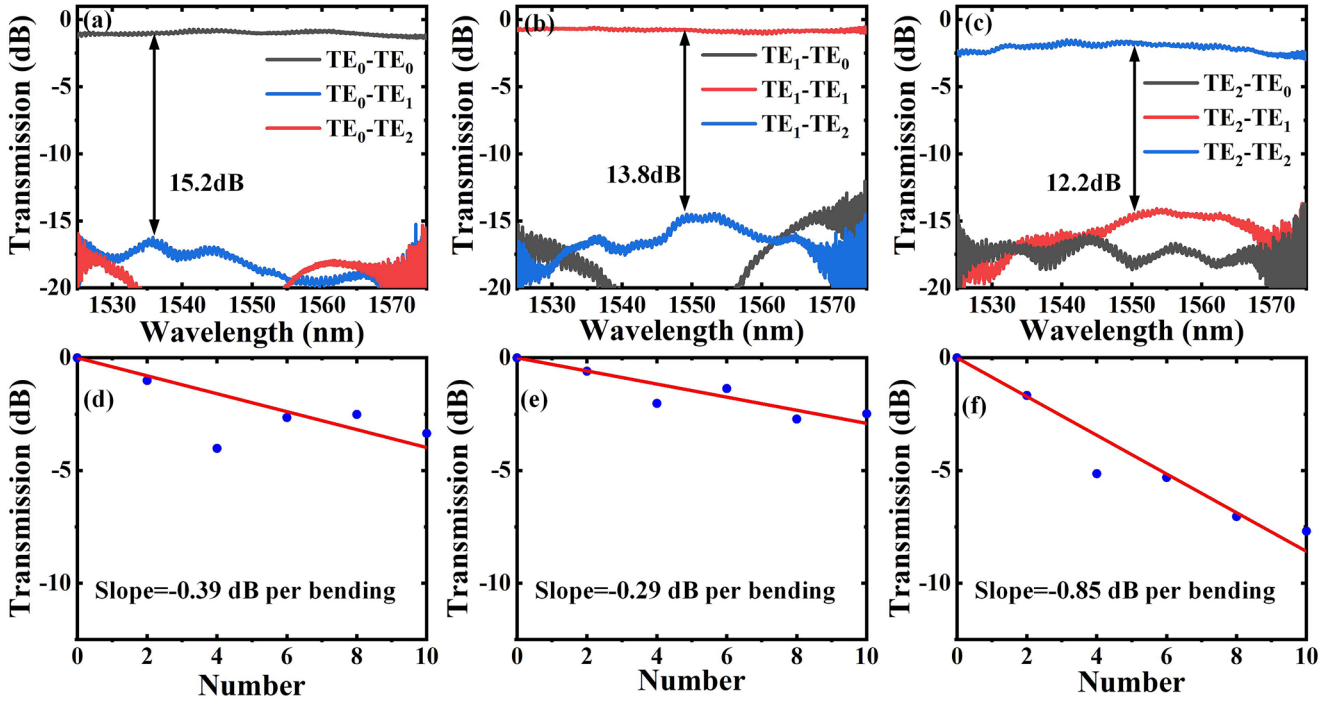

Figure 6. The measured transmission spectra for the a) TE_0, b) TE_1, and c) TE_2 input modes. Transmission as a function of the number of bends at the wavelength of 1550 nm for the d) TE_0, e) TE_1, and f) TE_2 input mode.

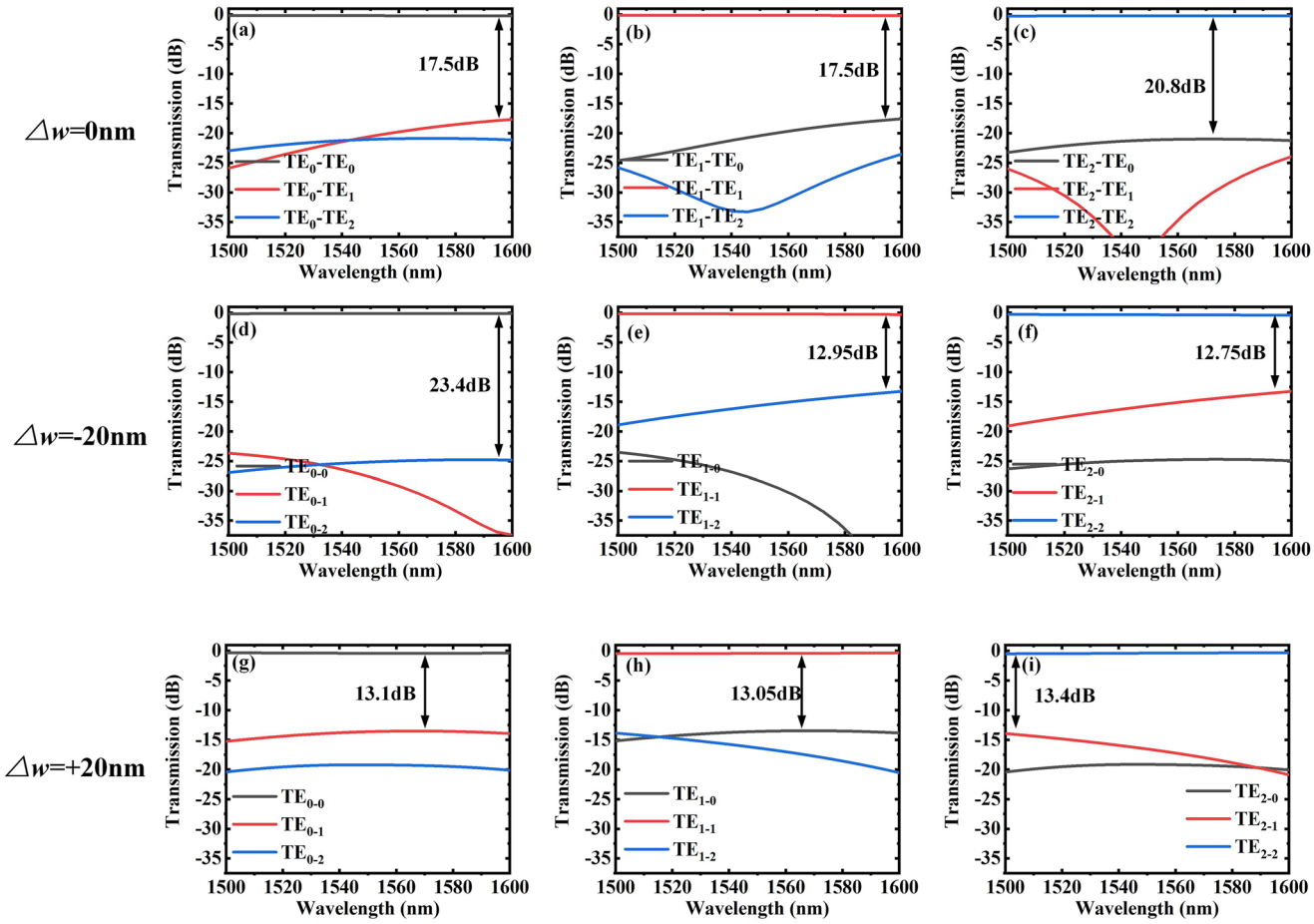

Figure 7. Transmission response of the proposed device to different fabrication variations of slot width. a–c) without fabrication variations, d–f) with −20 nm fabrication variation, and g–i) with +20 nm fabrication variation.

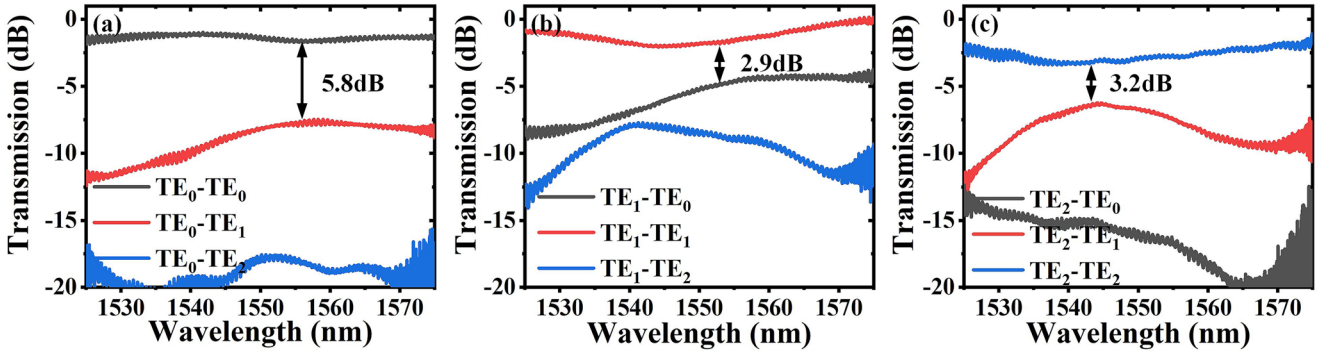

Figure 8. The measured transmission spectra of the multimode waveguide bends without air grooves for a) TE_0, b) TE_1, and c) TE_2 input modes.

4. Conclusion

In conclusion, we propose, simulate, and demonstrate a high-performance multimode waveguide bend with a radius of 120 μm and a waveguide width of 4.48 μm on the Si_3N_4 loaded LNOI platform, which can support the transmission of the TE_0, TE_1, and TE_2 mode with low loss and low crosstalk. Two air grooves with a width of 120 nm are used on the outer side of the bend to improve one mode overlap integral at the interface between the straight and bent waveguide to reduce transmission loss and inter-mode crosstalk of the multimode waveguide bend. The experimental results show that the insertion loss of the fabricated multimode waveguide bend is less than 0.85 dB at the wavelength of 1550 nm, and the crosstalk is less than −12.2 dB for two bends. Compared with multimode waveguide bends without any air grooves, our proposed device has lower transmission loss

and inter-mode crosstalk. Such bends are very attractive for constructing multimode PICs suitable for high-data-capacity communication applications.

Acknowledgements

The authors acknowledge the facilities and the scientific and technical assistance of the Micro Nano Research Facility (MNRF) and the Australian Microscopy & Microanalysis Research Facility at RMIT University. This work was performed in part at the Melbourne Centre for Nanofabrication (MCN) in the Victorian Node of the Australian National Fabrication Facility (ANFF). This work was supported by the National Key R&D Program of China (2021YFB2800103, 2022YFB2804202), National Natural Science Foundation of China (NSFC) (62075091), Open Fund of State Key Laboratory of Advanced Optical Communication Systems and Networks (2022GZKF007), and Australian Research Council (ARC) grants (DP190102773).

Conflict of Interest

The authors declare no conflict of interest.

Data Availability Statement

The data that support the findings of this study are available from the corresponding author upon reasonable request.

Keywords

lithium niobate on insulator, silicon nitride, multimode waveguide bends, microstructure

Received: November 12, 2022
Revised: December 14, 2022
Published online: January 31, 2023

[1] M. Levy, R. M. Osgood Jr., R. Liu, L. E. Cross, G. S. Cargill III, A. Kumar, H. Bakhru, *Appl. Phys. Lett.* **1998**, *73*, 2293.
[2] G. Poberaj, H. Hu, W. Sohler, P. Guenter, *Laser Photonics Rev.* **2012**, *6*, 488.
[3] A. Boes, B. Corcoran, L. Chang, J. Bowers, A. Mitchell, *Laser Photonics Rev.* **2018**, *12*, 1700256.
[4] Y. Qi, Y. Li, *Nanophotonics* **2020**, *9*, 1287.
[5] D. Zhu, L. Shao, M. Yu, R. Cheng, B. Desiatov, C. J. Xin, Y. Hu, J. Holzgrafe, S. Ghosh, A. Shams-Ansari, E. Puma, N. Sinclair, C. Reimer, M. Zhang, M. Lončar, *Adv. Opt. Photonics* **2021**, *13*, 242.
[6] S. Gao, M. Xu, M. He, B. Chen, X. Zhang, Z. Li, L. Chen, Y. Luo, L. Liu, S. Yu, X. Cai, *IEEE Photonics Technol. Lett.* **2019**, *31*, 1838.
[7] D. Guo, J. Liu, D. Zhang, *Opt. Laser Technol.* **2022**, *150*, 107972.
[8] P. Zhang, H. Huang, Y. Jiang, X. Han, H. Xiao, A. Frigg, T. G. Nguyen, A. Boes, G. Ren, Y. Su, Y. Tian, A. Mitchell, *Opt. Lett.* **2021**, *46*, 5986.
[9] M. Bahadori, Y. Yang, L. L. Goddard, S. Gong, *Opt. Express* **2019**, *27*, 22025.
[10] X. Han, Y. Jiang, A. Frigg, H. Xiao, P. Zhang, T. G. Nguyen, A. Boes, J. Yang, G. Ren, Y. Su, A. Mitchell, Y. Tian, *Laser Photonics Rev.* **2022**, *16*, 2100529.
[11] M. A. Baghban, J. Schollhammer, C. Errando-Herranz, K. B. Gylfason, K. Gallo, *Opt. Express* **2017**, *25*, 32323.
[12] J. Lu, M. Li, C. Zou, A. Al Sayem, H. Tang, *Optica* **2020**, *7*, 1654.
[13] B. Desiatov, A. Shams-Ansari, M. Zhang, C. Wang, M. Lončar, *Optica* **2019**, *6*, 380.
[14] C. Wang, M. Zhang, B. Stern, M. Lipson, M. Lončar, *Opt. Express* **2018**, *26*, 1547.
[15] X. Li, M. Wang, J. Li, K. Chen, *IEEE Photonics Technol. Lett.* **2019**, *31*, 1611.
[16] M. Piekarek, D. Bonneau, S. Miki, T. Yamashita, M. Fujiwara, M. Sasaki, H. Terai, M. G. Tanner, C. M. Natarajan, R. H. Hadfield, J. L. O'Brien, M. G. Thompson, *Opt. Lett.* **2017**, *42*, 815.
[17] M. R. Escalé, D. Pohl, A. Sergeyev, R. Grange, *Opt. Lett.* **2018**, *43*, 1515.
[18] E. Środa, J. Olszewski, W. Urbańczyk, *Appl. Opt.* **2022**, *61*, 1164.
[19] M. Cherchi, S. Ylinen, M. Harjanne, M. Kapulainen, T. Aalto, *Opt. Express* **2013**, *21*, 17814.
[20] X. Jiang, H. Wu, D. Dai, *Opt. Express* **2018**, *26*, 17680.
[21] F. Vogelbacher, S. Nevlacsil, M. Sagmeister, J. Kraft, K. Unterrainer, R. Hainberger, *Opt. Express* **2019**, *27*, 31394.
[22] M. Heiblum, J. Harris, *IEEE J. Quantum Electron.* **1975**, *11*, 75.
[23] S. Li, L. Cai, D. Gao, J. Dong, J. Hou, C. Yang, S. Chen, X. Zhang, *Photonics Res.* **2020**, *8*, 1843.
[24] H. Wu, C. Li, L. Song, H. K. Tsang, J. E. Bowers, D. Dai, *Laser Photonics Rev.* **2019**, *13*, 1800119.
[25] Y. Liu, K. Xu, S. Wang, W. Shen, H. Xie, Y. Wang, S. Xiao, Y. Yao, J. Du, Z. He, Q. Song, *Nat. Commun.* **2019**, *10*, 3263 .
[26] W. Chang, L. Lu, X. Ren, L. Lu, M. Cheng, D. Liu, M. Zhang, *IEEE Photonics J.* **2018**, *10*, 4501008.
[27] X. Han, Y. Jiang, A. Frigg, H. Xiao, P. Zhang, A. Boes, T. G. Nguyen, J. Yang, G. Ren, Y. Su, A. Mitchell, Y. Tian, *APL Photonics* **2021**, *6*, 086108.
[28] H. Huang, X. Han, A. Balčytis, A. Dubey, A. Boes, T. G. Nguyen, G. Ren, M. Tan, Y. Tian, A. Mitchell, *APL Photonics* **2022**, *7*, 106102.
[29] X. Han, L. Chen, Y. Jiang, A. Frigg, H. Xiao, T. Nguyen, A. Boes, J. Yang, G. Ren, Y. Su, A. Mitchell, Y. Tian, *Laser Photonics Rev.* **2022**, *16*, 2200130.
[30] Y. Jiang, X. Han, H. Huang, P. Zhang, A. Dubey, H. Xiao, M. Yuan, A. Frigg, T. G. Nguyen, A. Boes, Y. Li, G. Ren, Y. Su, A. Mitchell, Y. Tian, *Adv. Photonics Res.* **2022**, *3*, 2200121.
[31] Y. Tsuji, M. Koshiba, *J. Lightwave Technol.* **2000**, *18*, 618.